Res Nondestr Eval (1996) 8:101–123

Stress-Wave Displacement Polarizations and Attenuation in Unidirectional Composites: Theory and Experiment

B. Vandenbossche,[1] R. D. Kriz,[1] and T. Oshima[2]

[1]Department of Engineering Science and Mechanics, Virginia Polytechnic Institute and State University, Blacksburg, Virginia 24061-0219, USA
[2]College of Engineering, Kitami Institute of Technology, Kitami City, #090, Hokkaido, Japan

Abstract. The wave propagation mechanism of changes in displacement polarizations was studied in unidirectional graphite/epoxy composite materials. Change in Displacements can be large enough to cause a transition in the mode or displacement polarizations from longitudinal to transverse. These unusual mode transitions are a result of the peculiar elastic anisotropy observed in only a few crystals and unidirectional graphite/epoxy composities at high-fiber volume fractions. Theoretical calculation of these mode transitions were compared with experimental measurements. Mode transititons occur when the wave vector orientation is varied from 51.9° to 74.4° in unidirectional samples of T300/5208 graphite/epoxy composite with a 0.6°-fiber volume fraction. Energy flux deviation and particle displacement directions and amplitudes also were compared with theory. To show this mode transition, an attenuation study was performed. The attenuation coefficient, measured in units of reciprocal time, does not appear to depend on the wave vector orientation and the wave type (quasi-transverse and quasi-longitudinal waves) at 5-MHz frequency. But the attenuation coefficient, expressed in units of reciprocal length, does depend on the wave type and the wave vector orientation because the wave velocity is included in the calculation of this coefficient. Previous studies have focused on how anisotropy and attenuation influence the stress wave speed (eigenvalues), but in this study we focused more on how the same parameters influence the displacement polarizations (eigenvectors) of the same propagating waves. Because eigenvalues and their corresponding eigenvectors are both solutions of the same eigenvalue problem, more attention should be given to measurement of the eigenvectors.

List of Symbols

E_i = Young's moduli
G_{ij} = shear moduli
ν_{ij} = Poisson's ratios
C_{ij} = elastic-stiffness coefficients
C_{ijkl} = fourth-rank elastic-stiffness tensor
n_j = normalized wave vector (vector perpendicular to the plane wave)

ρ = mass density
δ_{ij} = Kronecker delta function
v = phase velocity
w_i = normalized particle displacement direction
J_i = energy flux vector
σ_{ij} = stress tensor
$\dot{u}_j$ = particle displacement velocity
u_I = incident wave of particle displacement amplitude
u_{QL} = quasi-longitudinal wave of particle displacement amplitude
u_{QT} = quasi-transverse wave of particle displacement amplitude
u_T = pure transverse of particle displacement amplitude
α_t = attenuation coefficients in s^{-1}
α_ℓ = attenuation coefficients in ℓ^{-1}
A_0 = maximum amplitude
$Q_{LL}(\theta)$ = longitudinal component of quais-longitudinal wave at θ
$Q_{LT}(\theta)$ = transverse component of quasi-longitudinal wave at θ
$Q_{TL}(\theta)$ = longitudinal component of quasi-transverse wave at θ
$Q_{TT}(\theta)$ = transverse component of quasi-transverse wave at θ
θ_{mt} = wave vector orientation corresponding to mode transition

Introduction

The industrial use of nondestructive evaluation (NDE) methods has greatly expanded since the second World War [1]. NDE methods have continued to develop and now can be classified into five major methods: radiographic, ultrasonic, magnetic, electrical, and penetrant [1]. Ultrasonic nondestructive evaluation is one of the most useful methods. It deals primarily with industrial and medical applications of both low-density and high-intensity ultrasonic energy [2]. To apply these methods, mechanics of wave propagation in materials must be understood. Considerable research has been performed on isotropic materials such as metals, ceramics, and polymers in which the mechanics of wave propagation are now well known.

Less is known about ultrasonic NDE in newer anisotropic materials. In the mid-1950s a new class of light-weight fiber-reinforced anisotropic materials with high strength and stiffness was developed for aerospace applications [3]. These materials are no longer homogeneous but are a heterogenous combination of two different materials: fiber and matrix. The fibers are typically strong, stiff, and resistant to heat; however, they are brittle. The matrix materials are typically ductile and have low density, but they have low stiffness and strength. Together these materials form an anisotropic composite that has the advantages of both materials, but it introduces a new source of wave attenuation due

to material heterogeneity. Wave propagation mechanics in these materials are typically more complicated than in homogeneous isotropic materials.

This article attempts to increase the understanding of ultrasonic wave propagation in unidirectional heterogeneous anisotropic composite materials. Typically, wave speed, energy flux deviations, and attenuation have been the primary parameters studied by various ultrasonic NDE methods. We extend our understanding of wave propagation mechanisms in anisotropic composites by studying displacement polarizations. The effect of signal attenuation caused by wave dispersion in heterogeneous materials is used to accurately measure changes in displacement polarizations. Several new and interesting physical mechanisms are observed when waves propagate in anisotropic materials. In fact, a mode transition occurs in the displacement polarizations, "mode transitions," from quasi-longitudinal to quasi-transverse when the wave vector orientation is varied with respect to the fiber orientation [4]. This mode transition will be verified experimentally.

Theory

Composite Materials

Composite materials are mostly anisotropic. Graphite/epoxy composites can be considered as linear, elastic, homogeneous (for long wavelengths), and anisotropic. A unidirectional graphite/epoxy material may be modeled to be linear, elastic, homogeneous, and transversely isotropic with five independent elastic constants: E_1, E_3, G_{12}, G_{13}, ν_{13} or as C_{11}, C_{33}, C_{44}, C_{12}, C_{13}. This coordinate axis system assigns the x_3-axis to the fiber axis.

For our material system of continuous parallel fibers we were concerned with the fiber spacing and the wavelength of the propagating wave. For the worst case we verified that the shortest wavelength is 350 μm (at 5 MHz) compared with the longest fiber spacing of 8 μm for our material system at a fiber volume fraction of 0.6. Hence our material appeared to be a well-mixed continuum of anisotropic material with respect to the frequencies used in this study. Although we can safely assume a homogeneous approximation for wave speed, wave amplitude is affected nonetheless by energy losses in a heterogeneous material and will be accounted for in the section on attenuation.

By considering the homogeneous linear elastic and transversely isotropic material properties, the elastic-stiffness constant tensor C_{ijkl} can be written as follows in contracted notation:

$$\begin{bmatrix} C_{11} & C_{12} & C_{13} & 0 & 0 & 0 \\ C_{12} & C_{11} & C_{13} & 0 & 0 & 0 \\ C_{13} & C_{13} & C_{33} & 0 & 0 & 0 \\ 0 & 0 & 0 & C_{44} & 0 & 0 \\ 0 & 0 & 0 & 0 & C_{44} & 0 \\ 0 & 0 & 0 & 0 & 0 & \frac{C_{11}-C_{12}}{2} \end{bmatrix}. \tag{1}$$

The material studied was a T300/5208 graphite/epoxy composite material with unidirectional fiber reinforcement. The fiber volume fraction of the material tested was 0.6. The average fiber diameter of the composite was about 8 μm.

Smith [5], Kriz and Stinchcomb [6, 7], and Datta et al. [8] calculated the composite material properties from the fiber and matrix properties, and verified them by using the properties measured by ultrasonic wave propagation. For the same material used in this study, Kriz and Ledbetter [4] showed that $C_{11} = 13.6$, $C_{33} = 144$, $C_{12} = 7.00$, $C_{13} = 5.47$, $C_{44} = 6.01$ GPa.

Wave Propagation Mechanisms

Wave Speed (Eigenvlaues) and Wave Displacement Polarization (Eigenvectors). Christoffel's equations are the equations governing the wave propagation mechanisms in solid materials:

$$(C_{ijk\ell}n_jn_k - \rho v^2\delta_{i\ell})w_\ell = 0, \qquad i, j, k, \ell = 1, 2, 3. \tag{2}$$

The solution to Christoffel's equation establishes the particle displacement wave types. The eigenvalues of this equation correspond to the phase velocities, whereas the eigenvectors are the particle displacement directions. Because of the physical properties of the material, the matrix $C_{ijk\ell}n_jn_k$ is symmetric and positive definite for any u_i, when $u_i(C_{ijk\ell}n_jn_k)u_\ell) \geq 0$ and equal to 0 only for $u_i = 0$. Therefore, the eigenvalues are real and positive, and the eigenvectors are orthogonal with respect to each other for distinct eigenvalues.

By knowing the material properties, the elastic-stiffness tensor, the mass density [4], and the components of the wave vector direction (normalized vector that is perpendicular to the plane wave), the theoretical phase velocities and particle displacement polarizations can be calculated.

For instance, when $\theta = 51.85°$, the eigenvalues ρv^2 are 4.95 Gpa, 66.6 GPa, and 10.9 GPa, where $n_i = [0, \sin(\theta), \cos(\theta)]$. Therefore, given the density [4], the corresponding phase velocities are:

$$\begin{aligned} v_T &= 1752 \text{ m/s} \\ v_{QL} &= 6431 \text{ m/s} \\ v_{QT} &= 2600 \text{ m/s}, \end{aligned} \tag{3}$$

and the normalized eigenvectors are:

$$w_1 = \begin{bmatrix} 1 \\ 0 \\ 0 \end{bmatrix}, \qquad w_2 = \begin{bmatrix} 0 \\ 0.1194 \\ 0.9928 \end{bmatrix}, \qquad w_3 = \begin{bmatrix} 0 \\ -0.9928 \\ 0.1194 \end{bmatrix}. \tag{4}$$

These three waves are labeled purely transverse (T), quasi-longitudinal (QL), and quasi-transverse (QT), respectively. Other wave speeds and particle displacements polarizations calculated by Kriz and Ledbetter [4] for different wave vector orientation clearly show this transition of displacement polarization from pure longitudinal to pure transverse on both QL and QT surfaces (see Fig. 1). The mode transition shown in Fig. 1 is for pure fiber elastic properties that were extrapolated using Hashin's Composite Cylinder Assemblage Model: $C_{33} = 235$ GPa, $C_{11} = 20.0$, $C_{12} = 9.98$, $C_{13} = 6.45$, $C_{44} = 24.0$ [4]; note that $C_{44} > C_{22}$.

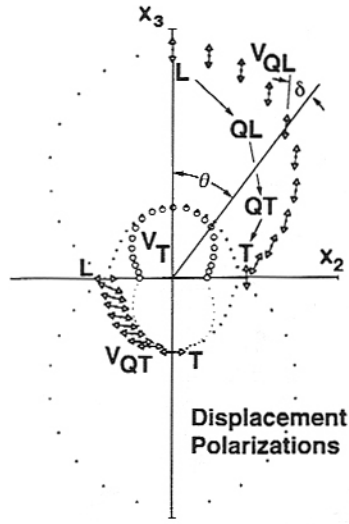

Fig. 1. Mode transitions of displacement polarizations on QL and QT wave surfaces for unidirectional graphite/epoxy at fiber volume fraction of 1.0: $L \rightarrow QL \rightarrow QT \rightarrow T$ on a V_{QL} surface, calculations: fiber elastic properties $C_{33} = 235$ GPa, $C_{11} = 20.0$, $C_{12} = 9.98$, $C_{13} = 6.45$, $C_{44} = 24.0$ [4]; note that $C_{44} > C_{11}$ [4].

The phase and group velocities are different from each type of wave (pure transverse, quasi-transverse, quasi-longitudinal). They also depend on the wave vector orientation and the elastic stiffness tensor. Typically, v_{QT} and v_T are smaller than v_{QL}. Although the frequencies of the three waves are generated by the same transmitter transducer, the quasi-transverse wavelength has to be smaller than the quasi-longitudinal wavelength because of different wave speeds. This was verified numerically by the computer simulation–visualization model of Kriz and Gary [9].

Energy Fluxes (Energy Bifurcation). The wave particle vibration directions, the plane wave equation, and the wave characteristics are known, but the energy flux of the waves is also important. The energy flux vector is

$$J_i = -\sigma_{ij}\dot{u}_j. \tag{5}$$

Substituting the expression for plane waves and general constitutive equations into the energy flux equation, an alternate expression for energy flux is

$$J_i = C_{ijk\ell} w_k k_\ell w_j \omega A^2 \sin^2(k_\ell x_\ell - \omega t). \tag{6}$$

Taking a time average over one period, the energy flux propagation direction reduces to

$$J_i = \frac{1}{2} C_{ijk\ell} w_k n_\ell w_j. \tag{7}$$

For different wave vector orientations, the energy flux deviation, Δ, calculation and measurement were calculated previously and measured by Kriz [4, 6, 9–12]. In addition,

Table 1. Particle displacement directions for different wave orientations.

Particle displacement directions (eigenvectors)			
Wave vector orientation (degrees)	Pure transverse wave	Quasi-longitudinal wave	Quasi-transverse wave
28	1 0 0	0 0.0445 0.999	0 −0.999 0.445
45	1 0 0	0 0.0864 0.9963	0 −0.9963 0.0864
51.85	2 0 0	0 0.1194 0.9928	0 −0.9928 0.1194
55	1 0 0	0 0.1296 0.9916	0 −0.9916 0.1296
70	1 0 0	0 0.3257 0.9455	0 −0.9455 0.3257

Prosser et al. [11] showed that the energy flux deviation shifts to a smaller angle when a load is applied to the sample. The shift depends on the applied load direction and amplitude.

To summarize, the wave propagation displacement and energy flux deviations in a unidirectional graphite/epoxy composite are shown in Fig. 2.

The computer simulation–visualization of these energy propagation directions using the finite differences method [9] clearly shows this propagation mechanism for different wave vector orientations.

Displacement Amplitudes (*Amplitude Bifurcation*). For v_{QL} and v_{QT}, similar particle displacement polarizations were calculated from Christoffel's equation for a wave vector orientation equal to 51.85°. Kriz and Heyliger [10] did the same calculation for wave vector orientations equal to 28°, 45°, 55°, and 70°. A summary of these results are listed in Table 1.

At the boundary surface between the transducer and the sample, the boundary conditions for stresses and displacement can be written as

$$\begin{aligned} \sigma_{ij}^{I} n_j - \sigma_{ij}^{II} n_j &= 0 \\ u_i^{I} - u_i^{II} &= 0. \end{aligned} \tag{8}$$

By considering the second condition, at the boundary the following relationship can be

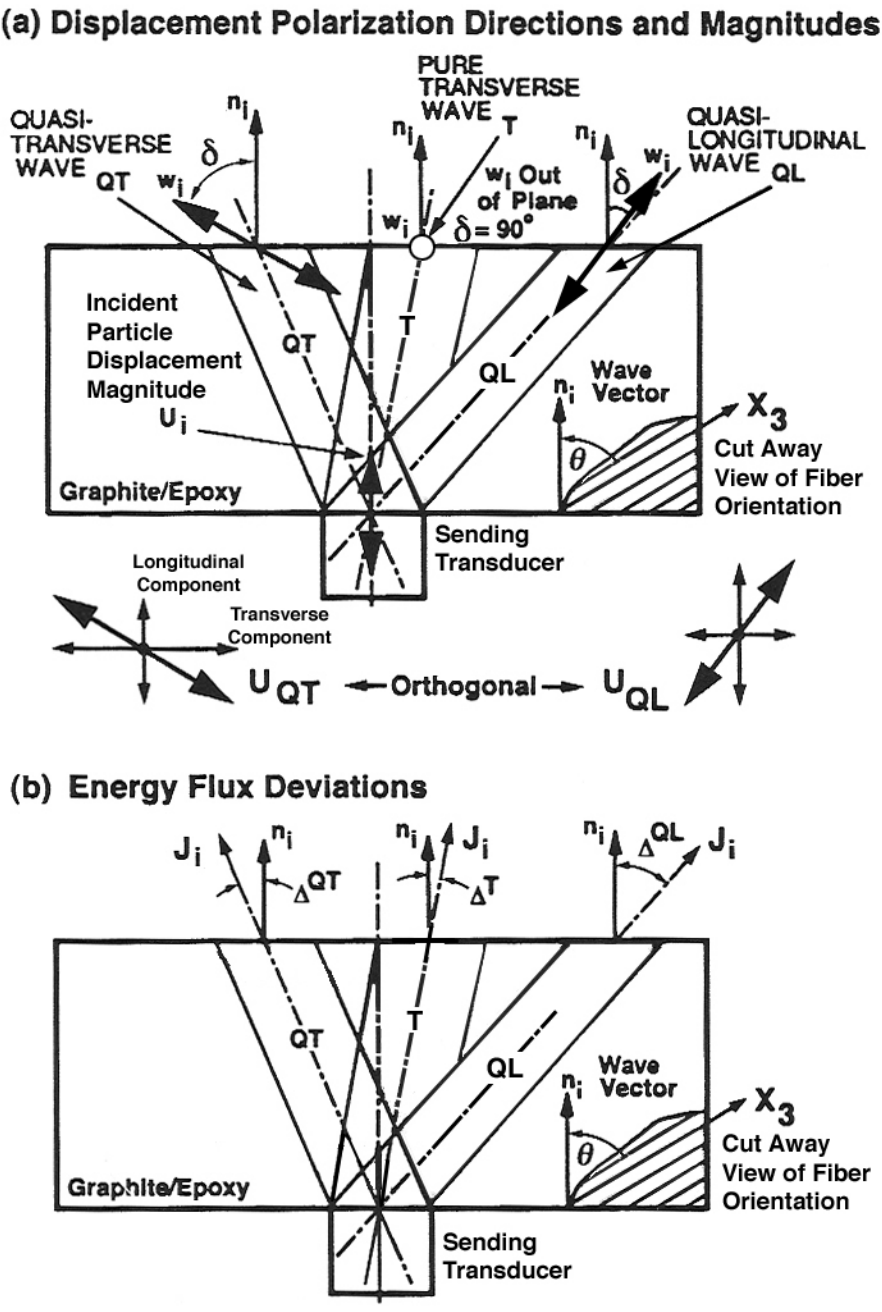

Fig. 2. Visual summary and definitions of wave propagation mechanisms that exist in anisotropic media: (a) QT and QL displacement polarizations and magnitudes are orthogonal and equal at $\theta = 51.85°$; (b) energy flux deviations also are influenced by anisotropy.

deduced:

$$\vec{u}_I - \vec{u}_{QL} - \vec{u}_T - \vec{u}_{QT} = 0. \tag{9}$$

Here the index I implies the incident wave where samples are cut such that incident angles, which are shown in Fig. 2, correspond to 28°, 45°, 51.85°, 55°, and 70° angles to the fiber orientation.

If the calculations are made at 51.85° wave vector orientation, then the results of Eq. (4) are combined with Eq. (9) to give:

$$\begin{bmatrix} 0 \\ 0.7864u_I \\ 0.6177u_I \end{bmatrix} - \begin{bmatrix} 0 \\ 0.1194u_{QL} \\ 0.9928u_{QL} \end{bmatrix} - \begin{bmatrix} u_T \\ 0 \\ 0 \end{bmatrix} - \begin{bmatrix} 0 \\ -0.9928u_{QT} \\ 0.1194u_{QT} \end{bmatrix} = \begin{bmatrix} 0 \\ 0 \\ 0 \end{bmatrix}, \tag{10}$$

which leads to

$$\begin{aligned} u_T &= 0 \\ u_{QL} &= 0.707u_I \\ u_{QT} &= 0.707u_I. \end{aligned} \tag{11}$$

Thus, the mode transition wave vector orientation is defined when the particle displacement amplitudes of the quasi-longitudinal and quasi-transverse waves are equal:

$$u_{QL} = u_{QT}. \tag{12}$$

This boundary condition also applies for 28°, 45°, 55°, and 70° wave vector orientations, and the results are compared in Fig. 3, where we have set the incident amplitude to unity.

In Fig. 3 the particle displacement amplitude of the quasi-longitudinal wave is larger than the quasi-transverse particle displacement when the wave vector orientation is below 51.85°. These same components are equal at the 51.85° wave vector orientation. Above 51.85°, the quasi-longitudinal particle displacement amplitude is smaller than the quasi-transverse particle displacement amplitude. Because the dominant mode of displacement transitions is from longitudinal to the transverse component, this behavior is referred to as a "mode transition."

Mode Transition. This mode transition also can be observed as a continuous transition by plotting the displacement deviation angle δ versus the wave vector orientation θ at various fiber volume fractions (see Fig. 4). The displacement deviation angle δ can be written as:

$$\delta = \cos^{-1}(n_i w_i); \tag{13}$$

see reference [4], where the wave vector n_i and the particle displacement deviation direction w_i depend on the wave vector orientation with respect to the fiber direction θ. Therefore, δ versus θ can be plotted as shown in Fig. 4. With this graph, mode transitions are identified at various wave vector orientation angles θ_{mt}. This graph also shows that mode transitions start at a fiber volume fraction of 0.3.

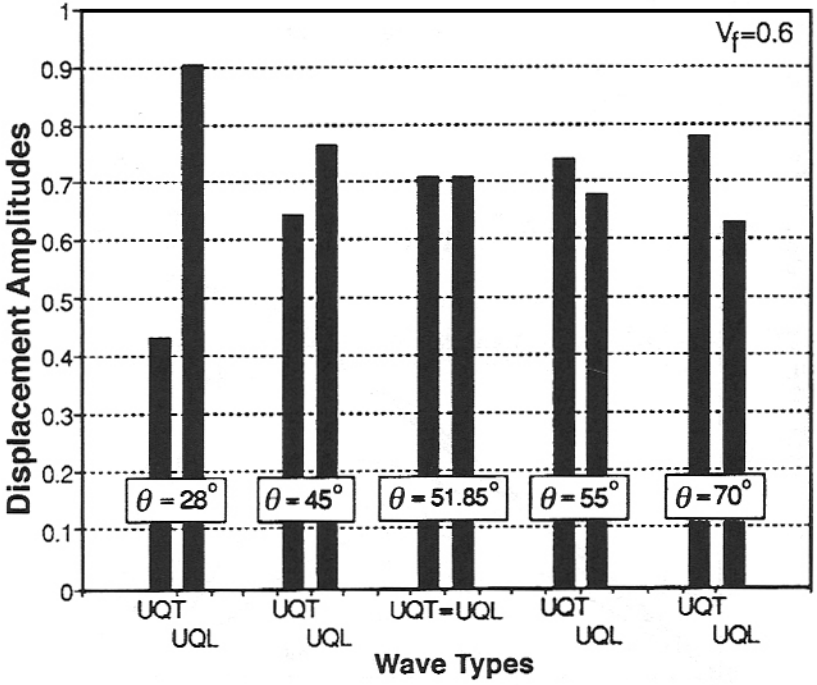

Fig. 3. Displacement magnitudes calculated at various wave vector orientations where the incident wave amplitudes is unity.

For fiber volume fractions between 0.3 and 0.96, the transition is partial, the quasi-transverse mode transitions back to the quasi-longitudinal mode and again becomes a purely longitudinal mode with increasing θ. Two mode transitions then are observed.

Because the elastic properties in reference [4], Fig. 4, are calculated using Hashin's Composite Cylinder Assemblage Model, properties can be extrapolated at fiber volume fractions greater than 0.91. Under these idealized conditions, mode transitions can be studied at fiber volume fractions greater than 0.96. Beyond 0.96, the second mode transition does not occur, and the quasi-transverse wave remains a QT wave and transitions into a purely transverse wave with increasing θ. There is only one known crystal, calcium formate, that displays this type of mode transition [13]. Indeed, this type of mode transition is rare, and hence the concept of a displacement polarization transformation is not common knowledge.

The objective of this study was to verify experimentally the mode transition that occurs in a graphite/epoxy composite at 0.6-fiber volume fraction. In order to allow a direct comparison with the results published in reference [4], the same material specimens that were tested in reference [4] were used in this study.

Because these transitions are rare, some precautions were taken because the labels generally given to the different waves do not necessarily correspond to the physical state of the wave. For instance, the quasi-transverse and quasi-longitudinal labels used in this study or in all previous publications are not always respectively quasi-longitudinal and

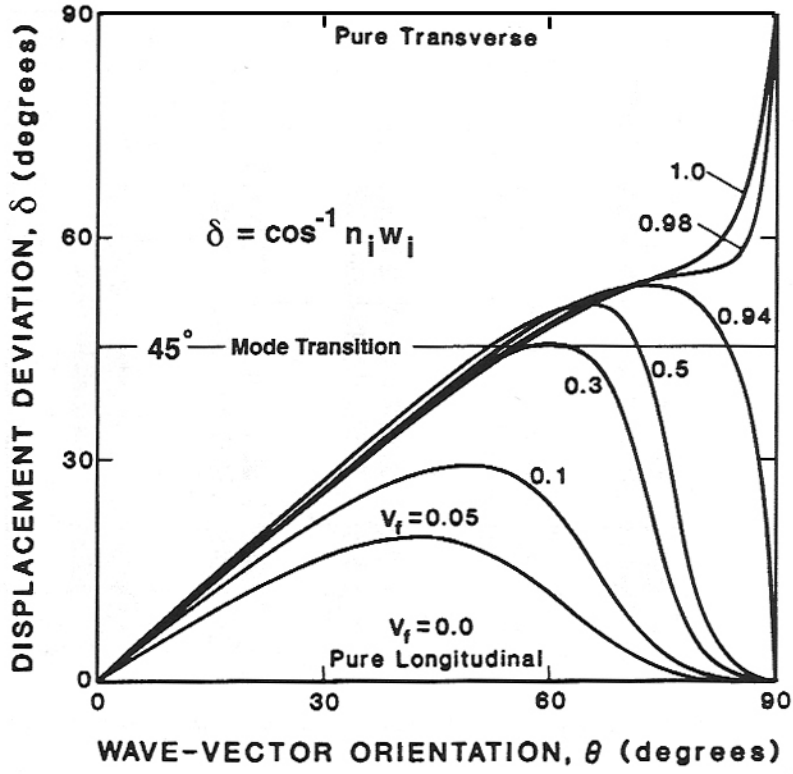

Fig. 4. Continuity of wave displacement polarization deviations from the wave normal at various wave vector orientations and fiber volume fractions show two types of transitions: type I, $L \rightarrow QL \rightarrow QT \rightarrow QL \rightarrow L$ and type II, $L \rightarrow QL \rightarrow QT \rightarrow T$.

quasi-transverse wave surfaces. Most authors use this type of notation [4, 6, 7, 9–12, 14–16] as a matter of habit, but this notation should not suggest that only one type of "mode" displacement polarization exists on a single surface.

The mode transition angle θ_{mt} can be calculated using Christoffel's equation (2) and the elastic-stiffness matrix, Eq. (1). The eigenvalue solutions are the roots of the characteristic equation derived from Christoffel's equation determinant

$$\begin{vmatrix} [C_{11}n_1^2 + C_{66}n_2^2 + C_{44}n_3^2] - \rho v^2, & [C_{12} + C_{66}]n_1n_2, & [C_{13} + C_{44}]n_1n_2 \\ [C_{12} + C_{66}]n_1n_2, & [C_{66}n_1^2 + C_{11}n_2^2 + C_{44}n_3^2] - \rho v^2, & [C_{13} + C_{44}]n_2n_3 \\ [C_{13} + C_{44}]n_1n_3, & [C_{13} + C_{44}]n_2n_3, & [C_{44}n_1^2 + C_{44}n_2^2 + C_{33}n_3^2] - \rho v_2 \end{vmatrix} = 0. \quad (14)$$

In our case the wave vector n_i has the following orientation with respect to the x_3-fiber axis:

$$\begin{bmatrix} 0 \\ \sin(\theta) \\ \cos(\theta) \end{bmatrix}. \quad (15)$$

To solve this determinant, mathematical software (*Mathematica*) was used [17]. The matrix in Eq. (14), the elastic-stiffness values, and the wave vector as a function of θ were substituted into *Mathematica*. The complete set of mathematical computations are given in reference [18]. The eigenvalues and corresponding eigenvectors were calculated as a function of θ. The $n_i w_i$ product then was calculated as a function of θ. At the mode transition, the particle displacement deviation is equal to 45°. Therefore, Eq. (13) becomes

$$n_i w_i = \cos 45^\circ = \frac{1}{\sqrt{2}} = 0.707107 \quad \text{at} \quad \theta = \theta_{mt}. \tag{16}$$

Because of the size of the equations, *Mathematica* was not able to solve for θ, therefore the half-interval method was used to solve for the two $n_i p_i$ products. The two mode transitions were solved and were equal to 51.85° and 74.4°, respectively.

Attenuation

When a stress wave passes through a material, a portion of its energy is absorbed or scattered; hence, the amplitude decreases. The attenuation is mainly due to absorption (also called *internal damping*), scattering (or *geometric dispersion*), diffraction, and beam spreading. The different attenuation mechanisms and their importance are discussed in reference [18]. Differentiating the various attenuation mechanisms was beyond the scope of this study. The collective effect of absorption, scattering, diffraction, and beam spreading were included into a single empirical value of attenuation. Certainly the dispersion of energy by diffraction had a significant influence on our attenuation coefficient.

The energy dissipation mechanism and the scattering losses from the beam can be expressed in terms of any one of these parameters which are collectively modeled by the attenuation factor (α), logarithmic decrement (δ), or dissipation factor (Q) [19]. Here, only the attenuation factor was used.

It is assumed that the transducer produces a plane stress wave that is attenuated as it propagates through the sample. The equation for the plane wave is

$$u_j(x_m, t) = A_j e^{i(k_m x_m - \omega t)}, \qquad j = 1, 2, 3, \tag{17}$$

where repeated m indices indicate summation.

An attenuated wave is obtained by assuming that the velocity is complex and that either the propagation vector or the frequency is complex.

For a complex propagation vector we have real and imaginary parts,

$$\begin{aligned} v &= v_1 + i v_2 \\ k &= k_1 + i\alpha^\ell, \end{aligned} \tag{18}$$

where the superscript on α^ℓ is not an index but represents the dimension of reciprocal length. The plane wave equation becomes

$$u_j(x_m, t) = A_j e^{-\alpha^\ell x_j} e^{i(k_m x_m - \omega t)}, \qquad j = 1, 2, 3. \tag{19}$$

Since α^ℓ was expressed in terms of distance x, α^ℓ has the dimension of a reciprocal length.

For a complex frequency we have

$$\begin{aligned} v &= v_1 + iv_2 \\ \omega &= \omega_1 + i\alpha^t. \end{aligned} \tag{20}$$

The plane wave equation becomes

$$u_j(x_m, t) = A_j e^{-\alpha^t t} e^{i(k_m x_m - \omega t)}, \qquad j = 1, 2, 3, \tag{21}$$

and α^t has the dimension of a reciprocal time.

Experimental Procedure

In order to verify experimentally the existence of a mode transition, it was necessary to use regression analysis on the shape of the received waveform and the log decay of multiple echos.

Curve-Fitting Signal Waveform

Experimental errors accounted for unexpected variations in the shape of the measured voltage as the transducer was moved in 0.5-mm increments along the top surface of the specimen shown in Fig. 2. The waveform shape was approximated by an appropriate function followed by a regression analysis of the second order.

The proposed function is

$$y = e^{-hx^2}, \tag{22}$$

where y is the measured receiver transducer voltage and x is the transducer position measured from the center line of the transmitting transducer.

The relationship below was used to match all of the data of the signal waveform:

$$y - y_0 = Ae^{-h(x-x_0)^2}. \tag{23}$$

By observing the data, it is obvious that when x is equal to infinity, y must be equal to zero; therefore, y_0 is also equal to zero. The final equation is

$$y = Ae^{-h(x-x_0)^2}. \tag{24}$$

This equation was written as a polynomial function to perform regression analysis on the experimental data. The equation above can be written as logarithms:

$$\ln(y) = \ln(A) - h(x - x_0)^2 \tag{25}$$

and

$$\ln(y) = -hx^2 + 2hx_0x + \ln(A) + hx_0^2. \tag{26}$$

By changing the variables,

$$\begin{aligned} Y &= \ln(y) \\ x &= x \\ a &= -h \\ b &= 2Hx_0 \\ c &= \ln(A) - hx_0^2, \end{aligned} \tag{27}$$

a second-order polynomial equation can be deduced:

$$Y = ax^2 + bx + c \tag{28}$$

The new parameters of this equation were calculated by multiple regression analysis. The coefficients a, b, and c are then known. The constants A, h, and x_0 can be determined from the following relationships:

$$\begin{aligned} h &= -a \\ x_0 &= -b/2a \\ A &= e^{(c-b^2/4a)}. \end{aligned} \tag{29}$$

A partial summary of results is presented in the Results and Discussion section. A complete summary is provided in reference [18].

Attenuation Measurement

Generally, a single short-duration pulse of high-frequency stress wave is introduced into the solid sample to measure the attenuation [19]. The attenuation can be measured on a parallel side sample, in order to achieve multiple echos [1]. Several echoes then are recorded and the parameters of the envelope equation are calculated [1].

The envelope equation is

$$A(t) = A_0 e^{-\alpha' t}. \tag{30}$$

If two echos are measured, the following equation can be used to calculate attenuation:

$$\alpha' = \frac{1}{t_2 - t_1} \ln\left[\frac{A(t_2)}{A(t_2)}\right]. \tag{31}$$

Otherwise, a linear regression is performed. This linear regression corresponds to the following envelope equation:

$$\ln(A(t)) = \ln(A_0) - \alpha' t. \tag{32}$$

Particle Displacement Direction Calculation

A transducer can measure either the transverse component of the wave (shear wave transducer) or the longitudinal component of the wave (longitudinal wave transducer).

These components will be measured and the particle displacement deviation will be calculated. Because orthogonality conditions exist between the displacement directions of the two waves, the following relationship can be written:

$$\delta = \tan^{-1}\left[\frac{Q_{LT}(\theta)}{Q_{LL}(\theta)}\right] = \tan^{-1}\left[\frac{Q_{TL}(\theta)}{Q_{TT}(\theta)}\right], \tag{33}$$

where a new notation is introduced to identify the longitudinal and transverse components of meaured voltage for the QL and QT waves:

$Q_{LL}(\theta)$ is the longitudinal component of the QL wave at θ,
$Q_{TL}(\theta)$ is the transverse component of the QL wave at θ.

The displacement deviation angle depends on either the ratio of a transverse component over a longitudinal component of the quasi-longitudinal wave or the opposite ratio of the quasi-transverse wave. Since these measurements are carried out by two different transducers, the measured amplitudes cannot be compared directly. To cancel the differences in characteristics between both transducers, such as piezoelectric properties, amplification factors, etc., differences between measurements corresponding to the same components will be calculated.

A reference point is required to make these calculations. This point corresponds to the mode transition. Since the mode transition occurs when the displacement deviation is equal to 45° ($\tan 45° = 1$) at this point, the transverse component must be equal to the longitudinal component for both quasi-longitudinal and quasi transverse waves. Since the quasi-transverse and quasi-longitudinal particle displacement amplitudes are equal at the mode transition wave vector orientation, the following relationship can be deduced:

$$Q_{LL}(\theta_{mt}) = Q_{LT}(\theta_{mt}) = Q_{TL}(\theta_{mt}) = Q_{TT}(\theta_{mt}). \tag{34}$$

Simple but lengthy relationships [18] then can be used to calculate the differences in each of the components of Eq. (34) such that plots of δ versus θ can be constructed to verify experimentally a mode transition.

Experimental Procedure

A pulse was launched into the graphite/epoxy composite by a 5-MHz transducer. This transducer was coupled to the composite sample with a Phenyl Salicylate couplant. The Sonotrace 30 couplant was used to measure the longitudinal component of the waves, and the SWC couplant was used to measure the transverse component of the waves. The receiving transducer, carrying a 0.180-Kg weight, next was placed on the receiving surface of the specimen. The pulser–receiver device was connected to the display device.

The amplitude of the waves was recorded for each position of the receiving transducer on the sample surface. A measurement was performed every 0.5 mm along the surface. Identical pulse characteristics (energy, response rate, and damping) were set up for all of the experiments. The sending pulse signal corresonds to a capacitive discharge. The received signal amplitude was the maximum amplitude of the signal. The fast Fourier transform of the signal was verified to make sure that the signal frequency corresponded

to the sending pulse signal. The frequency was constant, which suggets no dispersion, and our assumption of homogeneity was confirmed. The same weight was always used to keep a constant frequency and contact pressure. All of the experiments were carried out at the same room temperature ($\simeq 20°$).

Five samples with different fiber orientations were studied. The angles between the fiber orientation and the perpendicular line to the surface along which the pulse was sent were 28°, 45°, 51.85° (mode transition), 55°, and 70°, respectively. The accuracy of the angles was 0.1°. In fact, these angles correspond to the angle between the wave vector and the fiber orientation. Indeed, above 70° the measurement of the different waves became difficult because of the wave beam spreading and the interferences occurring between the three different waves. In order to obtain accurate measurements, the sending and receiving surfaces had to be parallel.

Results and Discussion

Measured Data

The experiments were repeated three times for the angles corresponding to 45° and 55° to increase the reliability of our results. Only one experiment was carried out on the sample having a wave vector orientation equal to 28° and 70°. The particle displacement amplitude versus position then was plotted; a complete set of figures are given in reference [18]. Figures 5a and b display the results for wave vector orientations equal to 45° and 55°. The transverse component cannot be compared to the longitudinal component directly because the transducer measuring the longitudinal component was different from the transducer measuring the transverse component. The curves corresponding to the wave vector orientation equal to 51.85° [18] show that the attenuation of the quasi-longitudinal wave if the assumption that these two waves should be equal is verified.

Fitting Data

The data then were fitted by the mathematical model previously defined. Then the calculated and measured particle displacement amplitudes were plotted on the same graph to verify the reliability of the mathematical model; a complete summary of the results is given in reference [18]. Figure 6 shows an example of these curves and demonstrates the accuracy of the regression analysis. The average correlation coefficient was 0.982.

In reference [18] the energy flux deviation also was measured and compared to the theoretical calculation. The energy flux deviation depends on the wave type (QL, QT, T) and on the wave vector orientation. Therefore, the geometrical attenuation is probably different for any wave type and wave vector orientation. In fact, all waves will travel through paths having different geomterical properties.

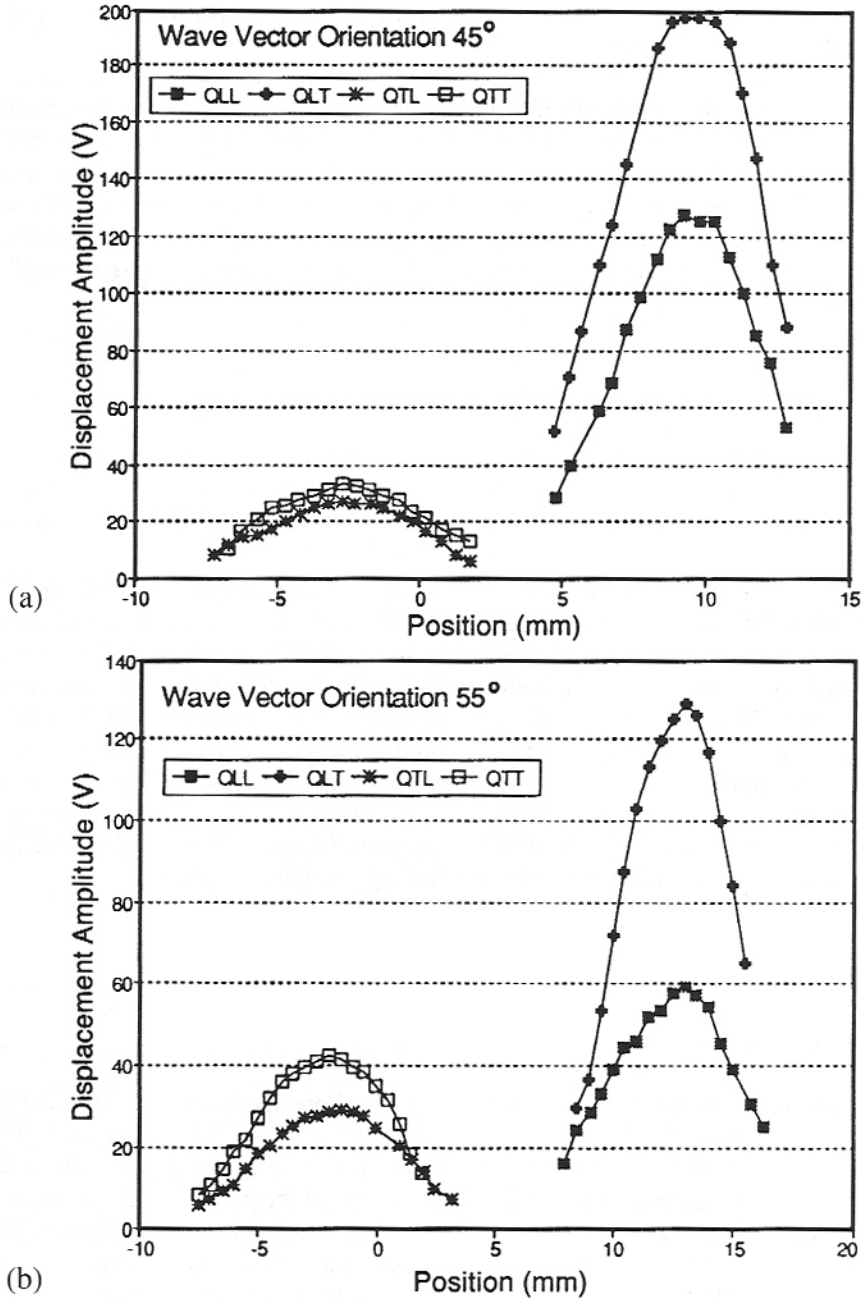

Fig. 5. Uncorrected (raw) displacement amplitudes at two wave vector orientations: (a) 45° and (b) 55°.

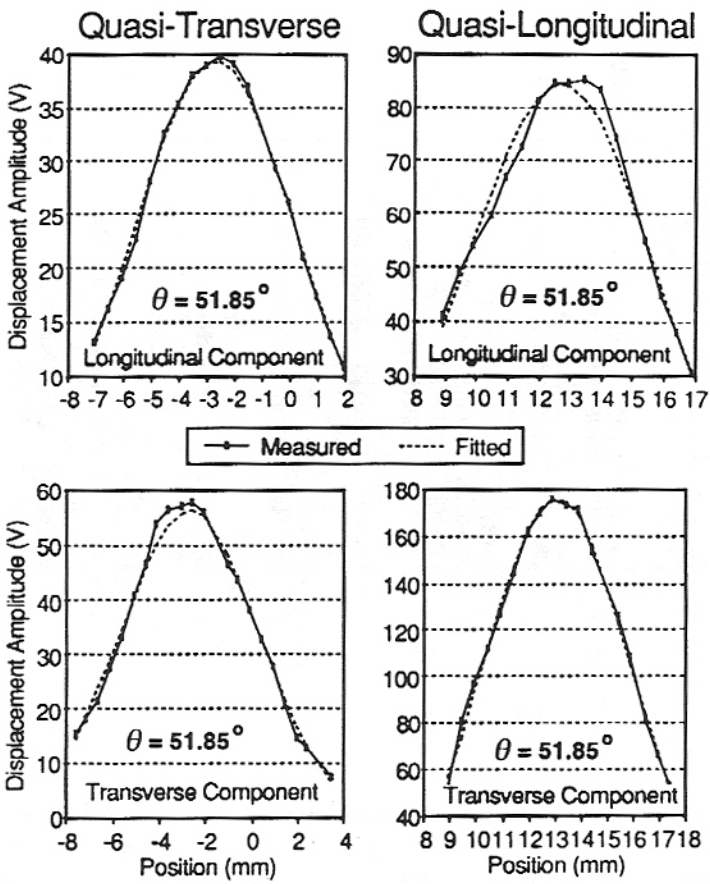

Fig. 6. Fitted data using regression analysis: average correlation coefficient 0.982 for all wave types.

Attenuation Calculation

For the same frequency, the quasi-transverse wavelength is different from the quasi-longitudinal wavelength because the phase velocities are different. When the wave vector orientation is equal to 51.85°, the different wavelengths are calculated and are equal to 0.350 mm, 1.286 mm, and 0.520 mm for the pure transverse, quasi-longitudinal, and quasi-transverse waves, respectively. The fiber diameter is about 8 μm. All of the wavelengths are greater than ten times the dimension of two fiber diameters. The wavelengths are large enough; therefore, the scattering of the waves is not the most important factor of the overall attenuation. The quasi-transverse wavelength and velocity are considerably smaller than the quasi-longitudinal ones; therefore, the quasi-transverse wave will oscillate more when both waves travel the same distance. Since the absorptions principally are due to losses in energy during these transformations, the absorption of the longitudinal component of the quasi-transverse wave also will be larger than the absorption of the longitudinal component of the quasi-longitudinal wave. The losses in

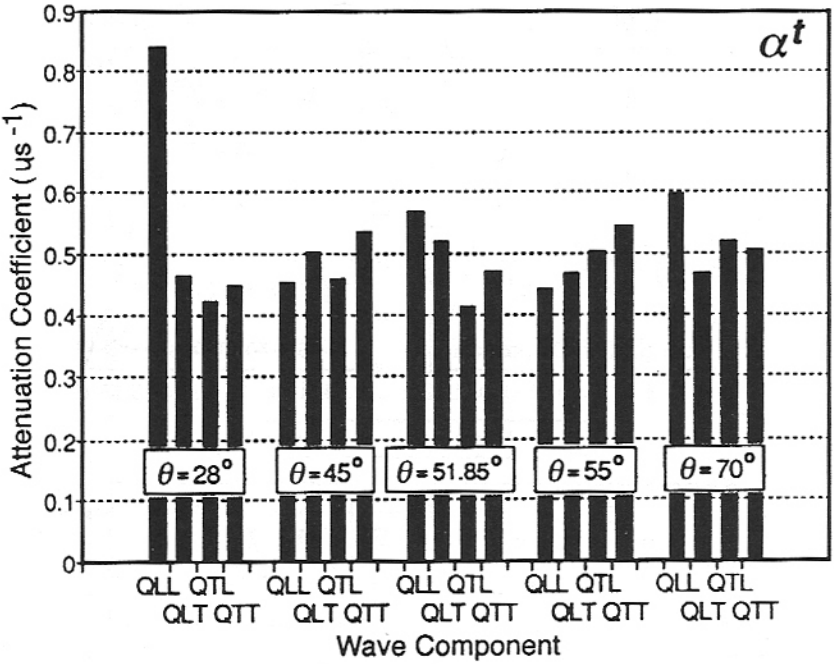

Fig. 7. Comparison of attenuation coefficients measured in reciprocal time for various wave components.

energy of the transverse components are probably due to the viscoelastic effect. Since the quasi-transverse wave will complete more full-cycle oscillations, the attenuation of the transverse component of the quasi-transverse wave will be larger than the attenuation of the transverse component of the quasi-longitudinal wave.

The attenuation factor can be expressed in two different units, either the reciprocal length (m^{-1}) or the reciprocal time (s^{-1}). The two attenuation factors are linked by the following relationship:

$$\alpha^t = v\alpha^\ell. \tag{35}$$

The attenuation factor was measured in the reciprocal time unit. To measure the attenuation factor, several echoes were recorded. The maximum number of echoes was always recorded, but, generally, only two echoes were observed on the display screen. The two first echoes then were observed and the attenuation coefficient was calculated [18].

If the different attenuation coefficients are compared, it can be deduced by observation in Fig. 7 that the attenuation coefficients are relatively constant; the average value is 0.489 μs^{-1}. A variance anaysis was performed with all of the data except the attenuation of the longitudinal component of the quasi-longitudinal wave. The wave type and the wave vector orientation were the analyzed parameters. If a 5% confidence is considered, the null hypothesis (all attenuation coefficients are equal) cannot be rejected for both parameters. No attenuation coefficient differs from the others; therefore, it can be con-

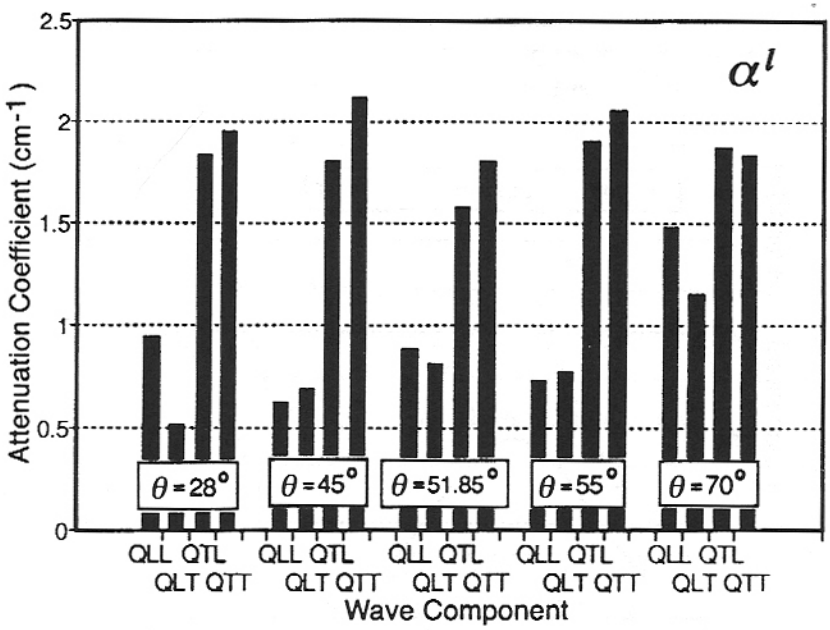

Fig. 8. Comparison of attenuation coefficients measured in reciprocal length for various wave components.

cluded that the attenuation coefficient expressed in reciprocal time units does not depend on the wave type and wave vector orientation. If the attenutation coefficient is expressed in the reciprocal length unit, the attenuation coefficient is not constant (see Fig. 8). The qusai-transverse attenuation is then more significant than the quasi-longitudinal attenuation. This is due to the smaller velocity and wavelength of the quasi-transverse wave. The attenuation, which is associated with reciprocal time, also depends on the wave vector orientation. This attenuation coefficient does not depend on the displacement magnitude; therefore, the longitudinal and the transverse components should have the same attenuation coefficient. This statement was verified for all of the wave vector orientations except for the 28° wave vector orientation.

Corrected Data

The attenuation occurring within the composite sample then was considered. The particle displacement amplitude corresopnding to a nonattenuated wave was calculated for all of the specimens in reference [18] and shown here for angles 45° and 55° in Figs. 9a and b, respectively, as was outlined earlier.

When the wave vector orientation is equal to 51.85°, the particle displacement amplitude of the quasi-transverse wave is equal to the particle displacement amplitude of the quasi-longitudinal wave. This equality of displacement amplitudes, Eq. (34), is now verified experimentally. For the other wave vector orientations, the particle displacement

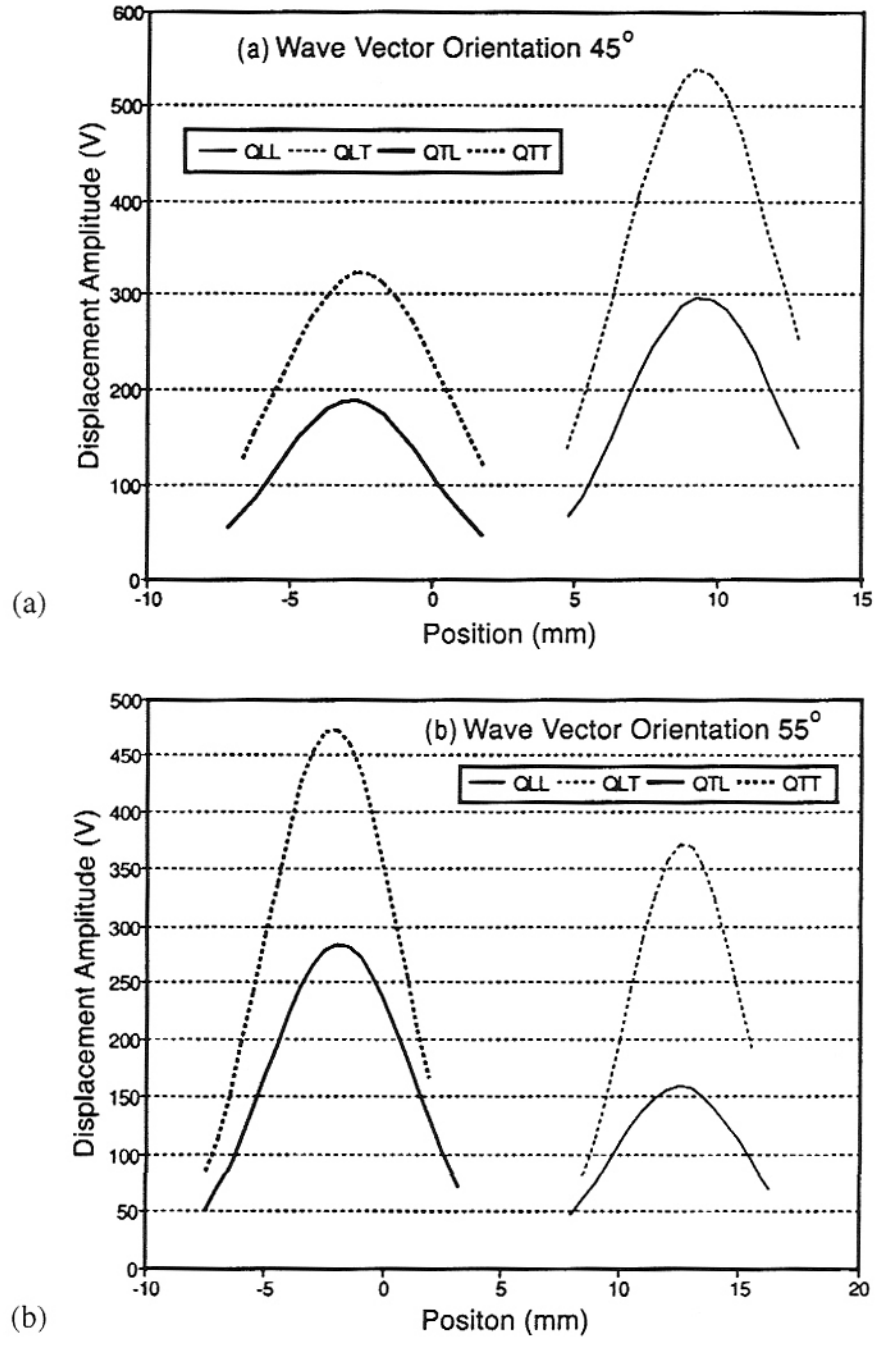

Fig. 9. Corrected displacement amplitudes at two wave vector orientations: (a) 45° and (b) 55°, showing a mode transition.

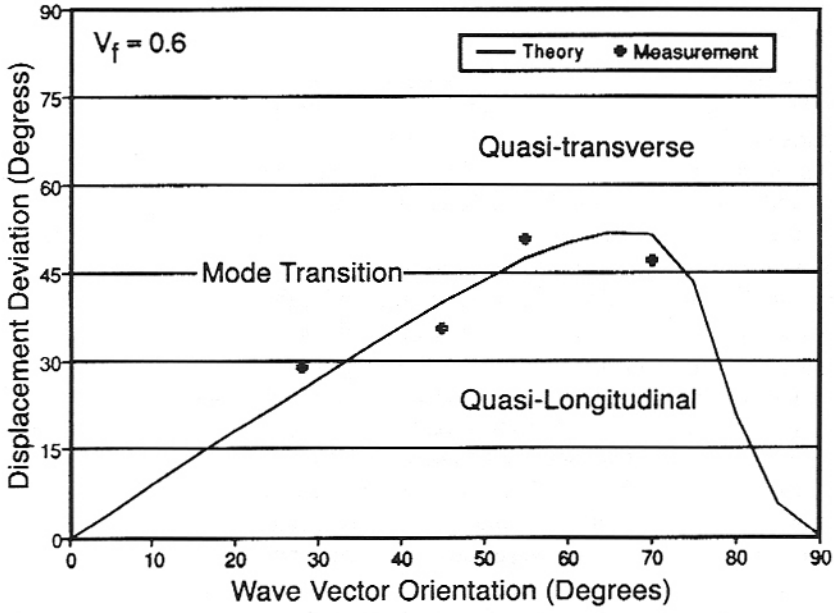

Fig. 10. Comparison of type I transition in displacement polarizations: theory and experiment.

direction cannot be deduced since the longitudinal component and the transverse component were measured by two different transducers. These curves show that the energy of the quasi-transverse wave is smaller than the quasi-longitudinal energy when the wave vector orientation is below 51.85° (the quasi-transverse particle displacement amplitudes are smaller than the quasi-longitudinal ones) [18]. Above 51.85°, the quasi-transverse wave energy is greater than the quasi-longitudinal wave energy [18]. This confirms the theoretical calculation.

Displacement Deviation (δ) Versus Wave Vector Orientation (θ)

Since the relationship in Eq. (34) has been verified experimentally, the differences between the wave components and the mode transition component now can be calculated, and then the particle displacement deviations (δ) can be calculated. These results were reported on the displacement deviation versus wave vector orientation plot and compared with theory (see Fig. 10).

The mode transition can be observed on this plot, even if the experimental data are not always close to the theoretical curves. The differences observed in Fig. 10 correspond to error from the measurement of different parameters and other approximations. Details of these differences are discussed in reference [18].

Conclusions

The objective of this study was to predict analytically and verify experimentally the mode transition of a stress wave propagating in a unidirectional graphite/epoxy composite. Comparison of theory and experiment is shown in Fig. 10.

All properties predicted by Christoffel's equation have been verified experimentally. Christoffel's equation predicts three different waves propagating through these materials. These waves are called the quasi-longitudinal, pure transverse, and quasi-transverse waves. The particle displacement directions of these waves are the eigenvector solutions to Christoffel's equation. The eigenvalues correspond to the phase velocity of these three waves. By imposing a frequency, the wavelength of the waves can be deduced. The energy flux calculation gives the directions in which the waves propagate through the material. Finally, the boundary conditions determine the particle displacement amplitudes of these three waves. Therefore, the various propagation properties in unidirectional anisotropic composites are known if we neglect the energy lost by attenuation of the material.

When the wave vector orientation changes with respect to the fiber orientation, a mode transition was observed for fiber volume fractions greater than 0.3. For fiber volume fractions above 0.94, the first wave transitions from pure longitudinal and becomes quasi-longitudinal, then quasi-transverse, and finally pure transverse with increasing wave vector orientation. The second wave follows the opposite path because of the orthogonality conditions.

For fiber volume fractions between 0.3 and 0.94, the first wave is longitudinal at 0° wave vector orientation, becomes quasi-longitudinal, quasi-transverse, quasi-longitudinal, and back to longitudinal in that order as the wave vector orientation increases. The second wave is first transverse, next quasi-transverse, then transitions to quasi-longitudinal, returns to quasi-transverse, and finally transverse when the wave vector orientation is increased. Two mode transitions occur in this case. For instance, at 0.6-fiber volume fraction, the mode transitions occur at 51.85° and 74.4° wave vector orientations, respectively. The first mode transition was observed experimentally. Five wave vector orientations (28°, 45°, 51.85°, 55°, and 70°) were studied. No wave vector orientation above 70° was investigated because of beam spreading. The wave amplitude predictions were confirmed experimentally. At the 51.85° wave vector orientation, the quasi-transverse and the quasi-longitudinal waves have the same particle displacement amplitude. Below this point, the particle displacement amplitude of the quasi-longitudinal wave is larger than the quasi-transverse amplitude. Above this point, the quasi-transverse wave particle displacement amplitude becomes larger. The energy flux deviation dependence on the wave vector orientation also was verified experimentally.

To make the experimental data comparable to the theory, the attenuation of the wave had to be considered. The attenuation was measured in units of reciprocal time. At 5 MHz, the attenuation coefficient in units of reciprocal time did not depend on the wave vector orientation and the wave type (quasi-longitudinal or quasi-transverse waves). The wavelength was considerably larger than the fiber diameter. But, when the attenuation coefficient was expressed in units of reciprocal length, the wave vector orientation and the wave type influenced the attenuation. This dependence is due to the fact that the velocity was included in the attenuation. The velocity depends on the wave vector orientation and the wave type.

With these new insights we have added to our understanding of wave displacement polarizations in anisotropic material systems. Future research should be focused on the study of different attenuation mechanisms.

Acknowledgments. The authors wish to thank the Virginia Institute of Material Systems for funding this study. They also thank Dr. E.G. Henneke and Dr. R.W. Hendricks for their helpful suggestions.

References

1. R. Haimshaw. *Nondestructive Testing*, Metallurgy and Materials Science Series, Arnold Edition (1987)
2. D. Ensminger. *Ultrasonics*, Second Edition, Marcel Dekker, Inc., New York and Basel, (1988)
3. G. Lubin. *Handbook of Composites*, Van Nostrand Reinhold, New York (1982)
4. R. D. Kriz and H. M. Ledbetter. In: *Recent Advances in Composites in United States and Japan* (ASTM STP 864), J. R. Vinson and M. Taya, eds., American Society for Testing and Materials, Philadelphia, pp. 661–675 (1985)
5. R. E. Smith. *J. Appl. Phys.* **43**(6): 2555–2562 (1972)
6. R. D. Kriz. *Mechanical Properties for Thick Fiber-Reinforced Composite Materials Having Transversely Isotropic Fibers*, Master's Thesis, VPI&SU, Blacksburg, VA (1976)
7. R. D. Kriz and W. W. Stinchcomb. *Exper. Mech.* **19**(2):41–49 (1979)
8. S. K. Datta, H. M. Ledbetter, and R. D. Kriz. *Int. J. Solids Structures* **20**(5):429–438 (1984)
9. R. D. Kriz and J. M. Gary. *Review of Progress in Quantitative Nondestructive Evaluation*, Vol. 9, 1990, pp. 125–132
10. R. D. Kriz and P. R. Heyliger. *Review of Progress in Quantitative Nondestructive Evaluation*, Vol. 8A, 1989, pp. 141–148
11. W. H. Prosser, R. D. Kriz, and D. W. Fitting. *IEEE 1990 Ultrasonics Symposium*, IEEE Press, pp. 961–964 (1990)
12. R. D. Kriz. In: *Solid Mechanics Research for Quantitative Nondestructive Evaluation*, Martin Nijhoff, pp. 389–395 (1987)
13. R. D. Kriz and H. M. Ledbetter. In: *Rheology of Anisotropic Materials*, C. Huet, D. Bourgoin and S. Richemond, eds., CR19 Coll, Paris 1984, Editions CEPADUES, Toulouse, 1986, pp. 79–92
14. D. W. Fitting, R. D. Kriz, and A. V. Clark. *Review of Progress in Quantitative Nondestructive Evaluation*, Vol. 88, 1989, pp. 1497–1504
15. B. Hosten. *J. Acost. Soc. Am.* **89**(6): 2745–2752 (1991)
16. R. A. Kline and Z. T. Chen. *Mat. Eval.* **46**:986–992 (1988)
17. S. Wolfram. *Mathematica*, Addison Wesley, Reading, Massachusetts (1988)
18. B. Vandenbossche. *Measurement of Ultrasonic Wave Mode Transition in Unidirectional Graphite/Epoxy Composites*, Master's Thesis, VPI&SU, Blacksburg, Virginia (1991)
19. R. Truell, C. Elbaum, and B. B. Chick. *Ultrasonic Methods in Solid State Physics*, Academic Press, New York, San Francisco, London (1969)